Journal of Theoretical Biology 421 (2017) 179–188

Contents lists available at ScienceDirect

Journal of Theoretical Biology

journal homepage: www.elsevier.com/locate/jtbi

Evaluating the influence of mechanical stress on anticancer treatments through a multiphase porous media model

Pietro Mascheroni[a], Daniela Boso[a], Luigi Preziosi[b], Bernhard A. Schrefler[c,*]

[a] Dipartimento di Ingegneria Civile, Edile ed Ambientale, Università di Padova, Via Marzolo 9, 35131 Padova, Italy
[b] Dipartimento di Scienze Matematiche, Politecnico di Torino, Corso Duca degli Abruzzi 24, 10124 Torino, Italy
[c] Institute for Advanced Study, Technische Universität München, Lichtenbergstraße 2, 85748 Garching bei München, Germany and Houston Methodist Research Institute, 6670 Bertner Ave, Houston, TX 77030, USA

ARTICLE INFO

Article history:
Received 20 November 2016
Revised 27 March 2017
Accepted 28 March 2017
Available online 6 April 2017

Keywords:
Cancer
Chemotherapy
Tumor spheroids
Mathematical model
Mechanical compression

ABSTRACT

Drug resistance is one of the leading causes of poor therapy outcomes in cancer. As several chemotherapeutics are designed to target rapidly dividing cells, the presence of a low-proliferating cell population contributes significantly to treatment resistance. Interestingly, recent studies have shown that compressive stresses acting on tumor spheroids are able to hinder cell proliferation, through a mechanism of growth inhibition. However, studies analyzing the influence of mechanical compression on therapeutic treatment efficacy have still to be performed. In this work, we start from an existing mathematical model for avascular tumors, including the description of mechanical compression. We introduce governing equations for transport and uptake of a chemotherapeutic agent, acting on cell proliferation. Then, model equations are adapted for tumor spheroids and the combined effect of compressive stresses and drug action is investigated. Interestingly, we find that the variation in tumor spheroid volume, due to the presence of a drug targeting cell proliferation, considerably depends on the compressive stress level of the cell aggregate. Our results suggest that mechanical compression of tumors may compromise the efficacy of chemotherapeutic agents. In particular, a drug dose that is effective in reducing tumor volume for stress-free conditions may not perform equally well in a mechanically compressed environment.

1. Introduction

A major hurdle to chemotherapy success is resistance of tumor cells to therapeutic agents. In general, resistance may arise as an intrinsic cellular response or as a result of drug treatment (Zahreddine and Borden, 2013). It is known that the presence of a low-proliferating cell population is one of the leading factors contributing to drug resistance in solid tumors (Mueller-Klieser, 2000; Trédan et al., 2007). In fact, several chemotherapeutic agents are effective against rapidly dividing cells. Moreover, as certain normal tissues display high rates of cellular divisions (such as the gut mucosal and bone marrow cells), there exists a toxicity limit determining the maximum administrable drug dose (Dawidczyk et al., 2014).

Such resistance mechanisms, dependent on the proliferative activity of tumor cells, are generally investigated *in vitro* through the use of three-dimensional cell aggregates, known as tumor spheroids (Vinci et al., 2012). Contrary to conventional monolayer cultures, tumor spheroids display heterogeneous cell populations, including quiescent and necrotic cells, together with resistant phenomena to different chemotherapeutic drugs (Mikhail et al., 2013). Cell quiescence results both from the lack of nutrients and growth factors within the tumor, and from adhesion interactions between cells of the same type. Indeed, cells from healthy tissues display a mechanism of "contact inhibition" that regulates proliferation in a crowded environment (Abercrombie and Ambrose, 1962). This mechanism allows the cells to stop proliferation as soon as certain cell densities are reached at a given site. Tumor cells exhibit an analogous behavior, even though to a significant lesser extent than their healthy counterpart, and with more relevance in three-dimensional cultures than in monolayers (St Croix et al., 1998).

The biochemical pathways underlying contact inhibition are still an active area of research. They are linked to adhesive interactions between neighboring cells, mediated by adhesion proteins such as cadherins. Moreover, these mechanisms include a series of proteins involved in cell cycle regulation. To this regard, the G1 checkpoint, also known as the restriction point (R), represents a fundamental step in the cell cycle, controlling cell commitment to mitosis (Planas-Silva and Weinberg, 1997). Regulation of this cell checkpoint depends on the retinoblastoma protein (pRb). In particular,

* Corresponding author.
E-mail address: bernhard.schrefler@dicea.unipd.it (B.A. Schrefler).

http://dx.doi.org/10.1016/j.jtbi.2017.03.027
0022-5193/

the hypo-phosphorylated form of pRb prevents progression from the G1 to the S phase of the cell cycle, inhibiting cell duplication. On the other hand, phosphorylation of pRb leads to its inactivation allowing the cell to undergo mitosis. Phosphorylation of pRb depends on cyclin-dependent kinases (cdks), which in turn are subject to the action of cyclins (Dietrich et al., 1997). Finally, the activity of the whole complex is further regulated by several inhibitor proteins, in particular the cyclin-dependent kinase inhibitors p27 and p16 (Hengst et al., 1994; Polyak et al., 1994). Interestingly, an over-expression of p27 has been observed following cell-cell contact in three-dimensional cultures, as compared to monolayers (St Croix et al., 1998, 1996; Xing et al., 2005). The adhesive interaction between cells inside tumor spheroids leads to upregulation of p27, which results in cell arrest in a quiescent phase of the cycle. Recently, the expression of p27 has been investigated through a series of experiments involving mechanical compression of three-dimensional cell aggregates (Delarue et al., 2014). Results show that a controlled compressive stress on tumor spheroids inhibits cell proliferation by an over-expression of p27, blocking the cancerous cells at the restriction point of the cell cycle.

At the beginning of this introduction, we have remarked that the presence of a non-proliferating cellular fraction has important consequences on the therapeutic efficacy of different chemotherapeutic agents. Notably, previous works have shown that a reduction in p27 expression in tumor spheroids could lead to better outcomes in terms of drug performance (St Croix et al., 1998, 1996; Xing et al., 2005). However, experiments quantifying the influence of mechanical stress on drug efficacy have still to be performed. Note that, interestingly, the compressive stresses that can be induced in tumor spheroids are of the same order of magnitude of those measured *in vivo* (Butcher et al., 2009; Fernández-Sánchez et al., 2015; Stylianopoulos et al., 2012), in the range of a few kPa.

Phenomena concerning the mechanisms of drug action, as well as the mechanical characterization of the state of a tissue, are difficult to investigate from a pure biological and biochemical framework. To this end, mathematical models provide a valuable tool for establishing which of the biophysical features of the tumor and the stroma are responsible for the observed behaviors. In the last years, several review papers discussing different approaches to cancer modeling have been published (Altrock et al., 2015; Byrne, 2010; Lowengrub et al., 2010; Preziosi and Tosin, 2009;. G. Sciumè et al., 2013). In particular, the first papers addressing the modeling of contact inhibition effects were (Chaplain et al., 2006; Galle et al., 2009). Some models describe the action of a therapeutic agent on tumor spheroids (see for example (Frieboes et al., 2009; Goodman et al., 2008; Ward and King, 2003)), whereas others take into account *in vivo* settings, as in (Hossain et al., 2012; Kim et al., 2013; Mpekris et al., 2015). There are also models addressing the effects of mechanical stress on tumor development, such as those in (Kim et al., 2011; Loessner et al., 2013; Stylianopoulos et al., 2012). However, to the authors' knowledge, there is a lack of mathematical models focusing on the interactions between anticancer agents and the mechanical environment surrounding the tumor.

The aim of this work is to develop a theoretical framework that is able to take into account these interactions, providing new insights into mechanics-mediated drug resistance. In the following, we specialize our study to tumor spheroids. We address the effects of a chemotherapeutic agent, supposed to target cell proliferation, on these cell aggregates. Then, we evaluate the influence of mechanical compression on treatment efficacy.

The remainder of this work is organized as follows. Section 2 describes the mathematical model; the governing equations are presented, together with the assumed constitutive relations and parameter values. In Section 3 we report the results of the model. We start from the effects of different drug concentrations on the spheroid growth curve. Then, we consider a range of mechanical pressures acting on the spheroid surface and investigate their interactions with the treatment. Finally, we test different mathematical expressions for the drug-induced cell death term. Section 4, at the end, presents some concluding remarks.

2. Mathematical model

2.1. Governing equations

We extend the work in (Mascheroni et al., 2016) to include the dynamics of a chemotherapeutic agent within an avascular tumor. In that work, we illustrated a mathematical model based on porous media mechanics to describe the growth of a tumor in the avascular stage. The model was further specialized to the case of tumor spheroids, and its numerical predictions were compared to experimental results concerning the mechanical compression of cell aggregates. Here, we start from the developed framework and the validated constitutive relations of our previous study to numerically investigate the effects of a therapeutic agent on the tumor. The tumor is modeled as a biphasic porous material, and the governing equations are derived from porous media theory. We denote by t the solid phase of the porous medium, constituted by tumor cells (TCs) and ECM. The interstitial fluid (IF) constitutes the fluid phase (ℓ), which permeates the pores of the cellular scaffold. In our description, TCs are divided into living (Lt) and necrotic (Nt) fractions. In addition, we assume that the IF carries a nutrient, namely oxygen (ox), and a drug (ch). We consider a saturated material, where the IF fills all the voids of the porous medium. This results in the saturation constraint:

$$\varepsilon^t + \varepsilon^\ell = 1 \tag{1}$$

where ε^α denotes the volume fraction of phase α ($\alpha = t, \ell$). The mass balance equations for the phases in the biphasic system are given by:

$$\frac{\partial\left(\varepsilon^t \rho^t\right)}{\partial t} + \operatorname{div}\left(\varepsilon^t \rho^t \boldsymbol{v}^t\right) = \underset{g}{\overset{\ell\to t}{M}} - \underset{d}{\overset{t\to\ell}{M}} \tag{2}$$

$$\frac{\partial\left(\varepsilon^\ell \rho^\ell\right)}{\partial t} + \operatorname{div}\left(\varepsilon^\ell \rho^\ell \boldsymbol{v}^\ell\right) = -\underset{g}{\overset{\ell\to t}{M}} + \underset{d}{\overset{t\to\ell}{M}} \tag{3}$$

where ρ^α is the true mass density and $\boldsymbol{v}^\alpha$ the velocity of the α phase ($\alpha = t, \ell$). Here $M_g^{\ell\to t}$ is the term responsible for mass exchange between IF and TCs, dependent on cell proliferation; $M_d^{t\to\ell}$ represents instead mass exchange between TCs and IF resulting from cell death and their following degradation. Oxygen and drug are described as species dissolved into the IF, and their mass balance reads:

$$\frac{\partial\left(\varepsilon^\ell \rho^\ell \omega^{ox}\right)}{\partial t} + \operatorname{div}\left(\varepsilon^\ell \rho^\ell \omega^{ox} \boldsymbol{v}^\ell\right) - \operatorname{div}\left[\varepsilon^\ell \rho^\ell D^{ox} \operatorname{grad}\left(\omega^{ox}\right)\right] = -\underset{ox}{\overset{ox\to t}{M}} \tag{4}$$

$$\frac{\partial\left(\varepsilon^\ell \rho^\ell \omega^{ch}\right)}{\partial t} + \operatorname{div}\left(\varepsilon^\ell \rho^\ell \omega^{ch} \boldsymbol{v}^\ell\right) - \operatorname{div}\left[\varepsilon^\ell \rho^\ell D^{ch} \operatorname{grad}\left(\omega^{ch}\right)\right] = -\underset{ch}{\overset{ch\to t}{M}} \tag{5}$$

where ω^β denotes the mass fraction of species $\beta = ox$, ch and D^β its diffusion coefficient. The terms $M_{ox}^{ox\to t}$ and $M_{ch}^{ch\to t}$ represent oxygen and drug uptake by TCs, respectively. We describe the evolution for living and necrotic TCs through the system:

$$\frac{\partial\left(\varepsilon^t \rho^t \omega^{Lt}\right)}{\partial t} + \operatorname{div}\left(\varepsilon^t \rho^t \omega^{Lt} \mathbf{v}^t\right) = -\varepsilon^t r^{Nt} + \underset{g}{\overset{\ell\to t}{M}} \tag{6}$$

$$\frac{\partial\left(\varepsilon^t\rho^t\omega^{Nt}\right)}{\partial t}+\operatorname{div}\left(\varepsilon^t\rho^t\omega^{Nt}\mathbf{v}^t\right)=\varepsilon^t r^{Nt}-\overset{t\to\ell}{\underset{d}{M}} \tag{7}$$

where we have denoted by ω^{Lt} and ω^{Nt} the mass fractions of living and necrotic cells, respectively. Here $\varepsilon^t r^{Nt}$ is an intra-phase mass exchange term, commonly denoted as reaction term, accounting for the transfer of TCs from living to necrotic. Note that, by summing (6) and (7) we obtain (2) assuming that:

$$\omega^{Lt}=1-\omega^{Nt} \tag{8}$$

Following porous media theory (Lewis and Schrefler, 1998; Pinder and Gray, 2008), the mechanical stress exerted on the solid phase is described through the effective stress tensor t^t_{eff} given by:

$$t^t_{\text{eff}}=t^t+\alpha_B p^\ell I \tag{9}$$

where I is the unit tensor, t^t the total stress tensor, p^ℓ is the fluid pressure in the interstitial fluid and α_B is Biot's coefficient defined by:

$$\alpha_B=1-\frac{K}{K_T}, \tag{10}$$

with K bulk modulus of the unsaturated skeleton and K_T bulk modulus of the solid phase. Then, we can state the linear momentum balance law for the tissue as (Lewis and Schrefler, 1998):

$$\operatorname{div}t^t=\operatorname{div}\left(t^t_{\text{eff}}-\alpha_B p^\ell I\right)=0 \tag{11}$$

Note that in (9) the tensile components of the stress tensors t^t and t^t_{eff} are assumed positive.

2.2. Constitutive relations

In (Mascheroni et al., 2016), constitutive relationships for the effective stress and the mass transfer terms have been formulated. In particular, we have assumed the following form for the effective stress:

$$t^t_{\text{eff}}=-\Sigma\left(\varepsilon^t\right)I \tag{12}$$

with $\Sigma(\varepsilon^t)$ given by:

$$\Sigma\left(\varepsilon^t\right)=\begin{cases}\alpha\left(\varepsilon^t-\varepsilon^t_0\right)^2\left[\dfrac{1-\varepsilon^t_n}{\left(1-\varepsilon^t\right)^\beta}-\dfrac{1}{\left(1-\varepsilon^t\right)^{\beta-1}}\right], & \text{if } \varepsilon^t>\varepsilon^t_0\\ 0, \quad \text{otherwise}\end{cases} \tag{13}$$

This pseudo-potential law describes cells that do not interact if their volume fraction is below a given threshold (ε^t_0). Otherwise, they start to interact and develop attraction forces as long as their volume fraction is below a control value (ε^t_n). Finally, if TCs become too densely packed exhibiting a high volume fraction, they start to repel each other. This behavior is schematized in Fig. 1. In the following we will denote by $\Sigma'(\varepsilon^t)$ the derivative of $\Sigma(\varepsilon^t)$ with respect to ε^t.

The mass exchange terms in Eq. (2) represent TC growth and death, respectively. The first term describes cell proliferation and depends on the transfer of mass between the IF and the living fraction of the tumor. Its expression, which is derived in (Mascheroni et al., 2016) for experiments involving compression of tumor spheroids, takes the form:

$$\overset{\ell\to t}{\underset{g}{M}}=\gamma^t_g\left\langle\frac{\omega^{ox}-\omega^{ox}_{crit}}{\omega^{ox}_{env}-\omega^{ox}_{crit}}\right\rangle_+\left(1-\delta_1\frac{\langle\Sigma\rangle_+}{\langle\Sigma\rangle_++\delta_2}\right)\omega^{Lt}\varepsilon^t \tag{14}$$

Here the coefficient γ^t_g accounts for oxygen uptake and for mass of IF that becomes tumor due to cell growth; ω^{ox}_{crit} is the critical mass fraction of oxygen, below which growth is inhibited, and

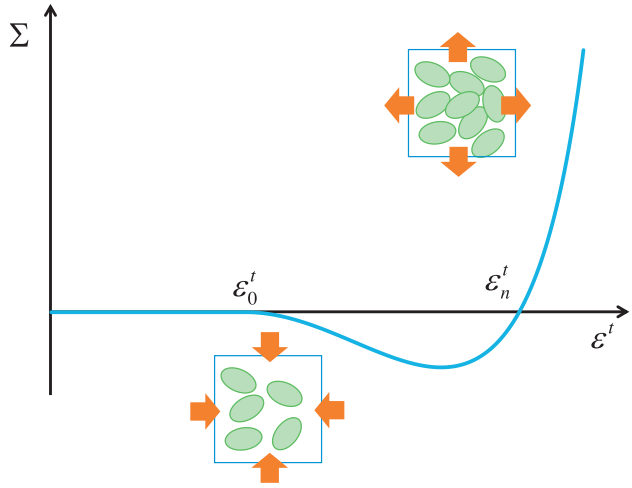

Fig. 1. Schematic for the stress function $\Sigma(\varepsilon^t)$, depicting the behavior of cells at different volume fractions.

ω^{ox}_{env} is the reference mass fraction of oxygen in the environment. The Macaulay brackets $\langle\cdot\rangle_+$ indicate the positive value of their argument: since the oxygen mass fraction ω^{ox} within the tumor can only be equal to or smaller than ω^{ox}_{env}, the brackets will return a number between one ($\omega^{ox}=\omega^{ox}_{env}$) and zero ($\omega^{ox}<\omega^{ox}_{env}$). The term in round squares describes growth inhibition by mechanical stress. The constants δ_1 and δ_2 (with $\delta_1<1$) regulate the action of mechanical stress on cell proliferation and, together with the term $\langle\Sigma\rangle_+$, model the inhibitory effect of compression on tumor cells proliferation (Cheng et al., 2009; Helmlinger et al., 1997; Montel et al., 2012).

The rate of TC death in Eq. (2) is given by:

$$\overset{t\to\ell}{\underset{d}{M}}=\overset{t\to\ell}{\underset{d,ly}{M}}+\overset{t\to\ell}{\underset{d,ch}{M}} \tag{15}$$

where the two contributions are related to cell lysis and drug action. In particular, the first term is given by:

$$\overset{t\to\ell}{\underset{d,ly}{M}}=\lambda^t_\ell\omega^{Nt}\varepsilon^t \tag{16}$$

where the coefficient λ^t_ℓ takes into account cellular degradation and mass conversion of necrotic cells into IF. The second term takes the form:

$$\overset{t\to\ell}{\underset{d,ch}{M}}=f_{ch}\lambda^t_{ch}\omega^{ch}\omega^{Lt}\varepsilon^t \tag{17}$$

Here λ^t_{ch} accounts for the rate of drug-induced cell death. The function f_{ch} is related to the mechanism of action of the drug that is considered. Since we are interested in drugs that target TC proliferation, we assume f_{ch} to depend on the growth term in (14):

$$f_{ch}(\omega^{ox},\Sigma)=\frac{M^{\ell\to t}_g}{\max\left(M^{\ell\to t}_g\right)}=\left\langle\frac{\omega^{ox}-\omega^{ox}_{crit}}{\omega^{ox}_{env}-\omega^{ox}_{crit}}\right\rangle_+\left(1-\delta_1\frac{\langle\Sigma\rangle_+}{\langle\Sigma\rangle_++\delta_2}\right) \tag{18}$$

where we highlight the dependence of f_{ch} on both the nutrient mass fraction ω^{ox} and the mechanical stress Σ. In this way, the drug is most effective on the TCs that are well nourished and not compressed. Note that, depending on the particular drug that is considered, different choices for f_{ch} are possible (for example, in this framework it is possible to simulate drugs targeting hypoxia or specific cellular species in the tumor).

The rate of necrosis of living tumor cells in Eq. (6) is described by:

$$\varepsilon^t r^{Nt} = \gamma_n^t \left\langle \frac{\omega^{ox}_{crit} - \omega^{ox}}{\omega^{ox}_{env} - \omega^{ox}_{crit}} \right\rangle_+ \omega^{Lt} \varepsilon^t \tag{19}$$

where the parameter γ_n^t regulates the rate of cell necrosis. The terms in the Macaulay brackets represent cell death by lack of nutrients.

During growth, TCs consume nutrients from the IF, a process that is described by the mass exchange term in Eq. (4):

$$\underset{ox}{M}^{ox\to t} = \gamma_0^t \frac{\omega^{ox}}{\omega^{ox} + c^{ox}} \omega^{Lt} \varepsilon^t \tag{20}$$

This expression accounts for the dependence of oxygen consumption on its local level in the tumor. The coefficients γ_0^t and c^{ox} represent the order of magnitude of oxygen uptake and the oxygen mass fraction at which consumption is reduced by half, respectively.

Finally, the mass transfer term related to drug uptake in Eq. (5) takes the form:

$$\underset{ch}{M}^{ch\to t} = \gamma_{ch}^t \omega^{ch} \omega^{Lt} \varepsilon^t \tag{21}$$

where we assumed the simplest kinetics for drug uptake (*i.e.* linear), with γ_{ch}^t accounting for the drug uptake rate by living TCs (Frieboes et al., 2009; Weinberg et al., 2007).

2.3. Model specialization to tumor spheroids

The equations of the model can be specialized to the case of tumor spheroids, following a procedure similar to the one in (Mascheroni et al., 2016). The resulting system for the TC volume fraction, necrotic mass fraction, and oxygen and drug mass fractions can be summarized as:

$$\frac{\partial \varepsilon^t}{\partial t} - \frac{1}{r^2}\frac{\partial}{\partial r}\left(r^2 \varepsilon^t \frac{k}{\mu^\ell} \Sigma' \frac{\partial \varepsilon^t}{\partial r} \right) - \frac{1}{\rho}\left(\underset{g}{M}^{\ell\to t} - \underset{d}{M}^{t\to \ell} \right) = 0 \tag{22}$$

$$\frac{\partial \left(\omega^{Nt} \varepsilon^t\right)}{\partial t} - \frac{1}{r^2}\frac{\partial}{\partial r}\left(r^2 \varepsilon^t \omega^{Nt} \frac{k}{\mu^\ell} \Sigma' \frac{\partial \varepsilon^t}{\partial r} \right) - \frac{1}{\rho}\left(\varepsilon^t r^{Nt} - \underset{d,ly}{M}^{t\to \ell} \right) = 0 \tag{23}$$

$$\frac{\partial \left[\left(1-\varepsilon^t\right) \omega^{ox} \right]}{\partial t} + \frac{1}{r^2}\frac{\partial}{\partial r}\left(r^2 \varepsilon^t \omega^{ox} \frac{k}{\mu^\ell} \Sigma' \frac{\partial \varepsilon^t}{\partial r} \right) - \frac{1}{r^2}\frac{\partial}{\partial r}\left[r^2 \left(1-\varepsilon^t\right) D^{ox} \frac{\partial \omega^{ox}}{\partial r} \right] + \frac{1}{\rho} \underset{ox}{M}^{ox\to t} = 0 \tag{24}$$

$$\frac{\partial \left[\left(1-\varepsilon^t\right) \omega^{ch} \right]}{\partial t} + \frac{1}{r^2}\frac{\partial}{\partial r}\left(r^2 \varepsilon^t \omega^{ch} \frac{k}{\mu^\ell} \Sigma' \frac{\partial \varepsilon^t}{\partial r} \right) - \frac{1}{r^2}\frac{\partial}{\partial r}\left[r^2 \left(1-\varepsilon^t\right) D^{ch} \frac{\partial \omega^{ch}}{\partial r} \right] + \frac{1}{\rho} \underset{ch}{M}^{ch\to t} = 0 \tag{25}$$

We have adopted spherical symmetry, and r is the radial coordinate over the spheroid radius. The parameters k and μ^ℓ are the intrinsic permeability of the cellular scaffold and the dynamic viscosity of IF, respectively. They arise by assuming Darcy's law for the relative velocity of the two phases (Mascheroni et al., 2016; G. Sciumè et al., 2013). Moreover, we take the phases to be incompressible and assign a common value for their densities, which we denote by the constant ρ. Note that this leads to $\alpha_B = 1$. Then, we model the growth of the spheroid as a free-boundary problem, where the interface constituted by TCs is a material surface for the TCs that moves with velocity v^t, given by:

$$\frac{dR}{dt} = v^t = -\frac{k}{\mu^\ell} \Sigma' \left. \frac{\partial \varepsilon^t}{\partial r} \right|_{r=R} \tag{26}$$

where R is the external radius of the spheroid. The closed form of the differential problem is then obtained by defining a proper set of boundary and initial conditions. In particular, regularity at the spheroid center requires:

$$\frac{\partial \varepsilon^t}{\partial r} = \frac{\partial \omega^{Nt}}{\partial r} = \frac{\partial \omega^{ox}}{\partial r} = \frac{\partial \omega^{ch}}{\partial r} = 0, \quad \text{in } r = 0, \tag{27}$$

while we enforce Dirichlet boundary conditions on the tumor external surface:

$$\varepsilon^t = \varepsilon^t_{ext}, \quad \omega^{Nt} = 0, \quad \omega^{ox} = \omega^{ox}_{env}, \quad \omega^{ch} = \omega^{ch}_{env}, \quad \text{in } r = R. \tag{28}$$

Finally, we assume the following initial conditions over the spheroid radius:

$$\varepsilon^t = \varepsilon^t_{ext}, \quad \omega^{Nt} = 0, \quad \omega^{ox} = \omega^{ox}_{env}, \quad \omega^{ch} = 0, \quad \text{on } 0 < r < R \text{ at } t = 0. \tag{29}$$

2.4. Model parameters

The parameters used in the model are listed in Table 1. Some of the values are taken from (Mascheroni et al., 2016), where the model results are compared to experimental data from tumor spheroids. In this work, we need to add the values for the parameters appearing in the equations governing drug transport and uptake. For these quantities we assume the values in (Frieboes et al., 2009), obtained for spheroids treated with Doxorubicin. Actually, the parameter governing drug-induced cell death, λ^t_{ch}, depends on the particular therapeutic agent and cell line that are considered. Here it is selected to produce a reasonable response of the model when the spheroids are subjected to the given drug concentrations. Note that, as it will be shown in Section 3.3, model results will not be significantly affected by this choice.

3. Results

3.1. Tumor spheroid growth in the presence of a drug

In this section we test the effects of a drug that targets cell proliferation in a three-dimensional cell aggregate. We consider first tumor spheroids that grow suspended in culture medium, subject to different drug concentrations. We assume drug concentration at spheroid boundary to start from zero and, following a ramp, to reach the final value ω^{ch}_{env} after 3 h

In Fig. 2, we show the evolution of the spheroid radius over time for different drug mass fractions (*i.e.* $\omega^{ch}_{env} = 0.086,\ 0.347,\ 1.391,\ 2.717 \times 10^{-7}$). Here, the arrow points in the direction of increasing ω^{ch}_{env}. We consider the normalized value of the spheroid radius, namely the ratio between the present value of the radius and the initial radius of the spheroid (200 μm in this case). The red line represents a spheroid grown in the absence of drug. We can distinguish between the first stages of growth, displaying an exponential/linear behavior, followed by a phase of growth saturation where the radius tends to a steady value. Low concentrations of drug do not alter the shape of the growth curve, whereas for high levels of the chemotherapeutic agent the spheroid starts to shrink and, for the highest value of ω^{ch}_{env}, growth is almost completely inhibited. This behavior closely resembles the growth curves obtained for example in (Kim et al., 2010; Mikhail et al., 2013). In the latter works, the authors analyzed the effects of different chemotherapeutics on tumor spheroids. In particular, Kim and colleagues compared the effects of free Doxorubicin and of a

Table 1
Parameters used in the model.

Parameter	Value	Unit	Reference
ω_{env}^{ox}	7.7×10^{-6}	(-)	(Mueller-Klieser et al., 1986; Mueller-Klieser and Sutherland, 1982)
c^{ox}	1.48×10^{-7}	(-)	(Casciari et al., 1992a, 1992b)
γ_0^t	3.0×10^{-4}	kg/(m^3 · s)	(Casciari et al., 1992a, 1992b)
β	0.5	(-)	(Byrne and Preziosi, 2003)
ε_n^t	0.8	(-)	(Byrne and Preziosi, 2003)
ε_0^t	1/3	(-)	(Byrne and Preziosi, 2003)
k	1.8×10^{-15}	m^2	(Netti et al., 2000)
μ^ℓ	1.0×10^{-3}	Pa · s	(G. Sciumè et al., 2013b)
D^{ox}	3.2×10^{-9}	m^2/s	(G. Sciumè et al., 2013b)
ρ	1.0×10^3	kg/m^3	(G. Sciumè et al., 2013b)
ω_{crit}^{ox}	2.0×10^{-6}	(-)	(Mascheroni et al., 2016)
γ_g^t	5.4×10^{-3}	kg/(m^3 · s)	(Mascheroni et al., 2016)
γ_n^t	1.5×10^{-1}	kg/(m^3 · s)	(Mascheroni et al., 2016)
λ_ℓ^t	1.15×10^{-2}	kg/(m^3 · s)	(Mascheroni et al., 2016)
α	1.0×10^5	Pa	(Mascheroni et al., 2016)
ω_{env}^{ch}	$8.696 \div 271.76 \times 10^{-9}$	(-)	(Frieboes et al., 2009)
D^{ch}	9.375×10^{-14}	m^2/s	(Frieboes et al., 2009)
γ_{ch}^t	1.157×10^{-2}	kg/(m^3 · s)	(Frieboes et al., 2009)
λ_{ch}^t	5.0×10^4	kg/(m^3 · s)	(-)

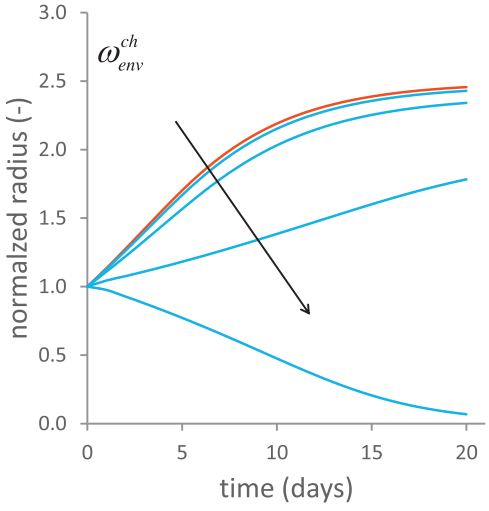

Fig. 2. Effect of different drug concentrations on spheroid growth. The red line refers to a spheroid grown in the absence of drug. The other lines are for $\omega_{env}^{ch} = 0.086,\ 0.347,\ 1.391,\ 2.717 \times 10^{-7}$.

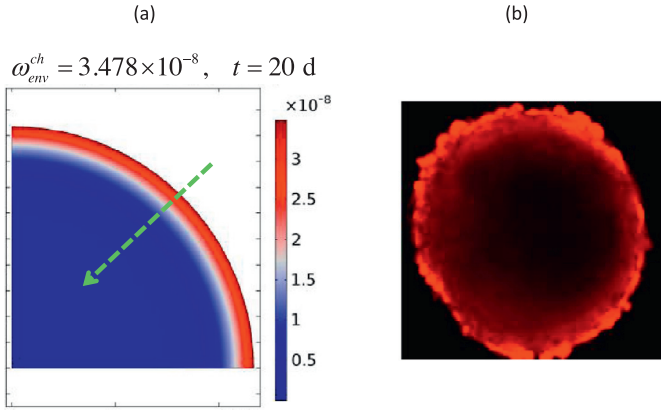

Fig. 3. (a) Drug mass fraction inside the spheroid at day 20 and for $\omega_{env}^{ch} = 3.478 \times 10^{-8}$. The arrow points to the direction of decreasing drug mass fraction. (b) CLSM image of a SH-SY5Y spheroid incubated with free Doxorubicin. Note the distribution pattern similar to the one predicted by the model. Reprinted from (Wang et al., 2013), with permission from Elsevier.

formulation of the same drug encapsulated in micelles. They characterized Doxorubicin activity both in monolayer cell cultures and in three-dimensional tumor spheroids, composed of human cervical carcinoma cells (SiHa). Following a similar procedure, Mikhail and coworkers established a series of assays to evaluate the *in vitro* efficacy of Docetaxel micelles and Taxotere® in tumor spheroids from human cervical (HeLa) and colon (HT29) cancer cells. Both the works reported the evolution of the spheroid growth curves as a function of time and of the incubated drug. Similarly to Fig. 2, they showed that low exposures to the drugs do not alter significantly the time evolution of the spheroid volumes, whereas higher drug concentrations were able to completely inhibit tumor growth.

Fig. 3a shows the drug mass fraction inside the spheroid for an intermediate value of ω_{env}^{ch}, at the end of the simulation. Note the steep gradient of drug appearing from the boundary towards the center of the cell aggregate. In this case, the therapeutic agent can exert its effect only over the outermost region of the spheroid. This phenomenon arises both as a consequence of poor diffusion of the drug molecules inside the spheroid and of the fact that the drug is uptaken by duplicating cells that are mainly located toward the periphery (due to contact inhibition). Interestingly, similar results are obtained in the experimental literature (see for example (Gong et al., 2015; Wang et al., 2013)), analyzing the penetration of free drug into a spheroid. In particular, Gong and colleagues presented a novel spheroid culture method based on agarose scaffolds to provide a robust platform for *in vitro* drug evaluation. They tested this method to produce spheroids from human breast adenocarcinoma cells (MCF-7), and characterized tumor response to Doxorubicin in terms of drug penetration, cell cycle distribution, cell apoptosis and gene expression. On the other hand, Wang and coauthors studied the cellular uptake, tumor penetration, biodistribution and antitumor activity of different Doxorubicin-conjugated nanoparticles by using tumor spheroids from a human neuroblastoma cell line (SH-SY5Y). They showed that a particular nanoparticle formulation was able to significantly improve the efficiency of Doxorubicin in the spheroids, resulting in efficient cell killing. Both the works evaluated the drug distribution inside the spheroids through confocal laser scanning microscopy (CLSM), and reported images from representative spheroid cross-sections. The authors observed a time-dependent drug penetration in the tumor, and highlighted that the distribution of free Doxorubicin was strictly limited to the outer cell layers of the spheroids. One image from the work in (Wang et al., 2013) showing poor drug penetration in the spheroid is re-

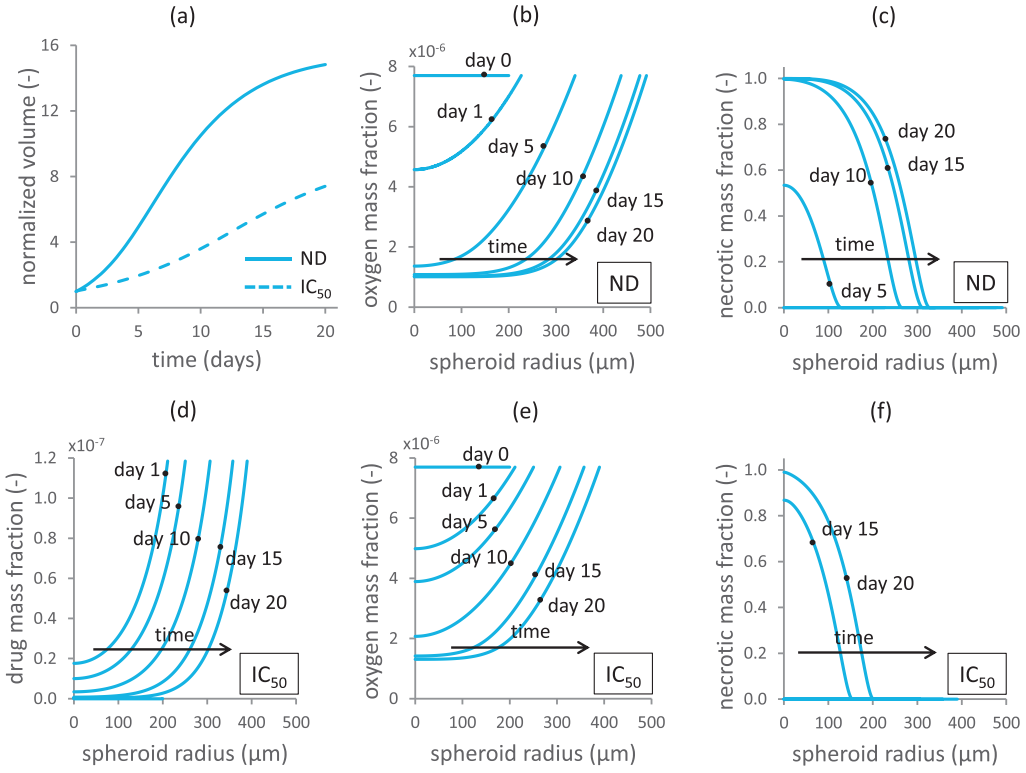

Fig. 4. Comparison between a spheroid grown without an external drug (ND) and one treated with a drug mass fraction equal to IC_{50}. (a) Time evolution of the spheroid volumes. (b), (c) Spatiotemporal variation of oxygen mass fraction and necrotic mass fraction over the spheroid radius for the ND case. (d) Spatiotemporal evolution of the drug mass fraction over the spheroid radius. (e), (f) Spatiotemporal variation of oxygen mass fraction and necrotic mass fraction over the spheroid radius for the IC_{50} case.

ported in Fig. 3b, displaying a pattern similar to the one obtained from our model.

In the following, we look for the value of drug mass fraction that is able to provide a reduction of 50% in spheroid volume at the end of the simulation (day 20, in this case). This value is usually identified with the label IC_{50}, for "half maximal inhibitory concentration" (Curtis et al., 2016). We find a value of $\omega_{env}^{ch} = 1.185 \times 10^{-7}$, which we will denote from now on with IC_{50}. The growth curve relative to this drug mass fraction is shown in Fig. 4a, where we report the evolution of the normalized volume (*i.e.* the ratio between the spheroid volume and its initial volume) over time. The evolution of oxygen mass fraction over the spheroid radius is represented in Fig. 4b. Note the steep oxygen gradients at later times of the simulation, from the spheroid boundary towards its interior. The necrotic mass fraction of TCs is displayed in Fig. 4c. A necrotic population appears after a few days from the beginning of the simulation and gives rise to a necrotic core at later days. Both Figs. 4b and 4c refer to a spheroid not treated with the drug, whereas the second row of Figs. (4d-f) pertains to a spheroid grown in the presence of a drug with a mass fraction equal to IC_{50}. The drug mass fraction over the spheroid radius is presented in Fig. 4d. Note that, after a few days from the beginning of the simulation, the therapeutic agent is mainly distributed over the spheroid periphery. Fig. 4e shows the oxygen mass fraction in the drug-treated spheroid. We can observe a behavior similar to the one in Fig. 4b, but this time over a smaller spheroid. Finally, the necrotic mass fraction in a spheroid subjected to the drug is shown in Fig. 4f. Compared to Fig. 4c, here the necrotic core is less extended and appears at later times in the simulation. This may be due to a smaller mass fraction of LTCs that can undergo necrosis, deriving from LTC killing by the chemotherapeutic agent.

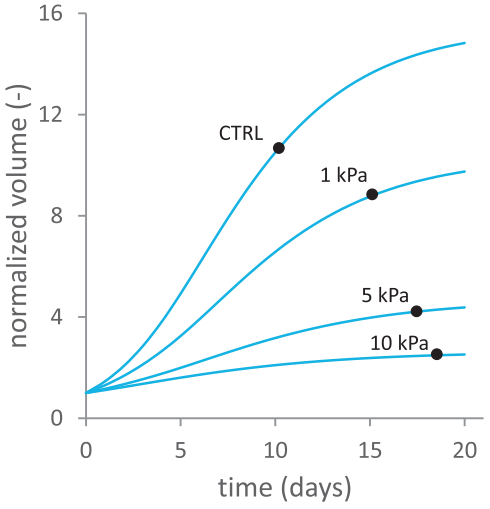

Fig. 5. Normalized volumes of spheroids grown under different external mechanical pressures.

3.2. Effect of mechanical compression on drug efficacy

In (Mascheroni et al., 2016), we investigated the effects of an external mechanical pressure on the growth curves of tumor spheroids. Fig. 5 report these previous findings, in terms of the evolution of the normalized volumes of spheroids subjected to different compressive stresses. We consider three compression levels, ranging from 1 kPa to 10 kPa. The growth of the most compressed spheroid shows a 7-fold reduction when compared to the control case (grown in the absence of an external stress). Note that the inhibitory effect of compressive stresses is included in the equations

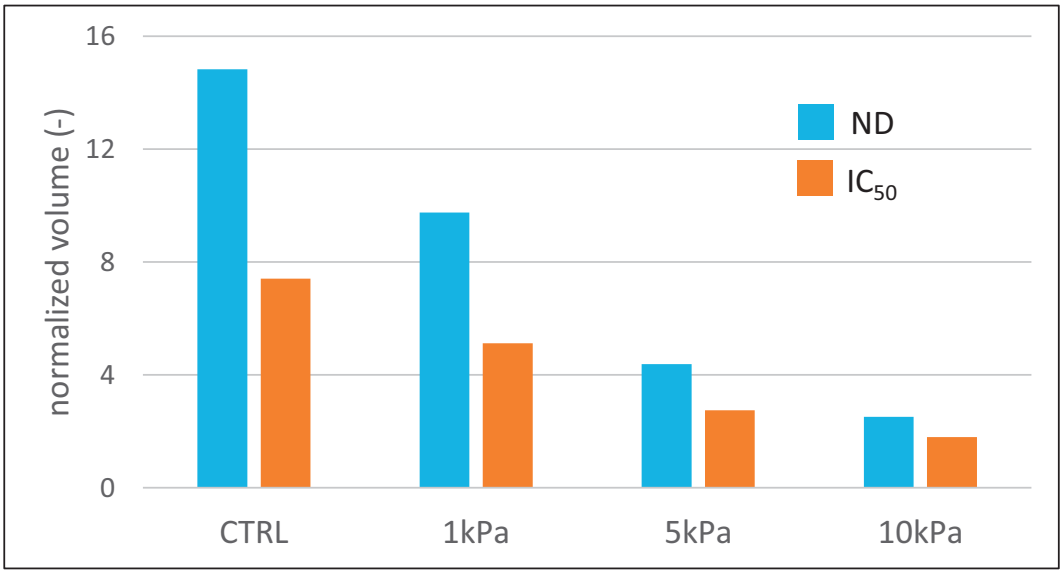

Fig. 6. Comparison of the normalized volumes of spheroids subject to different mechanical stress, grown in the absence of drug (ND) or subject to a drug concentration of IC_{50}.

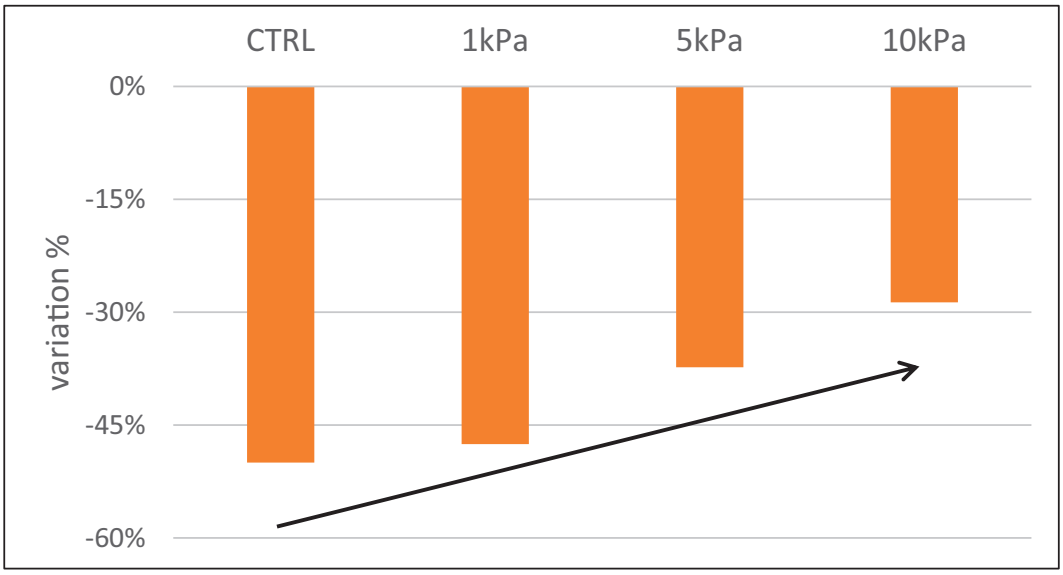

Fig. 7. Variation in spheroid volume due to the action of a chemotherapeutic drug, at a concentration of IC_{50}, for different external mechanical pressures. As shown by the arrow, the efficacy of proliferation targeting drugs is less effective for higher tumor compressions, because of stress inhibition of growth.

through the constitutive relation in (14). We make use of these results to test our newly introduced framework for drug transport and uptake in the spheroid. In particular, we apply the same external mass fraction of drug (IC_{50}) to each of the compression tests. Then, we check for variations in spheroid volumes with respect to the case with no drug added to the culture medium (Figs. 6 and 7). Fig. 6 compares the normalized volumes of spheroids undergoing different compressive stresses. We test spheroids in the absence (ND) or presence (IC_{50}) of a chemotherapeutic drug. Both the series, ND and IC_{50}, exhibit the same decreasing trend, although with a slower volume reduction for drug-treated spheroids. The variation between the two volumes for each compressive condition is shown in Fig. 7. According to the definition of IC_{50}, the control case displays a 50% reduction in volume. Interestingly, the series exhibit a percentage variation decreasing with the extent of mechanical compression, as highlighted by the black arrow. The case undergoing maximum compression shows a reduction of about 30% in volume reduction. The observed behavior arises as a consequence of a lower proliferation index within the spheroid. In fact, mechanical stress inhibits cell proliferation via Eq. (14) of the model, providing smaller values for the growth term as compression increases. The values in Fig. 7 can be plotted against the external mechanical compression, as shown in Fig. 8. Note that, as the efficacy of the drug depends on the mechanism for growth inhibition by Eq. (18), and since the latter saturates for increasing external pressures, a similar saturation trend could be observed in the Figure. Since our discussion is based on drugs that target cell duplication, growth inhibition is responsible for a cell population over which the therapeutic agent is less effective. Note that this effect could be relevant for *in vivo* applications: a drug concentration that is known to be effective in a particular regime (such as 3D cultures) could not provide the same results when the tumor is subjected to mechanical compression. Moreover, since several drug screenings are eval-

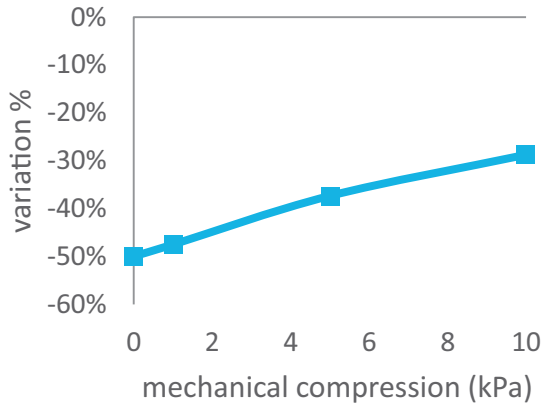

Fig. 8. Spheroid volume variation as a function of external mechanical compression. The spheroids are subjected to the action of a chemotherapeutic agent at a concentration of IC_{50}. Note the saturation effect at higher compressions, which follows from the expression for growth inhibition.

uated on monolayer cultures, such effects arising from a full three-dimensional setting may be overlooked (Friedrich et al., 2009).

3.3. Response of the model for different forms of the drug-induced death term

To confirm that model results are not biased by the particular choice of the term in (17), we test different mathematical expressions accounting for drug-induced cell death. The simplest hypothesis, assumed in (17), considers cell death to be proportional to the local amount of drug. In the following, we will refer to this case as the "linear" one. We introduce two additional relationships, given by:

$$\underset{d,ch}{\overset{t\to\ell}{M}} = f_{ch}\frac{m_1\omega^{ch}}{\omega^{ch}+m_2}\omega^{Lt}\varepsilon^t \tag{30}$$

$$\underset{d,ch}{\overset{t\to\ell}{M}} = f_{ch}p_1\left(\omega^{ch}\right)^{p_2}\omega^{Lt}\varepsilon^t \tag{31}$$

In (30), we assume a dependence of the Michaelis–Menten type; in (31) the assumed relationship takes the form of a power law. All laws however maintain through f_{ch} the same dependence on the duplication law, having in mind drugs that act on proliferating cells. Note that, as the functional dependence on the local drug concentration changes, these relations give rise to new values for the inhibitory concentration IC_{50}. We report the new IC_{50} and the values for the parameters that characterize the above expressions in Table 2. Once the new forms for the drug-induced cell death term are implemented into the model, we perform the same numerical tests of the previous section to analyze the coupled effect of drug action and mechanical compression. In Fig. 8, we display the variation in terms of spheroid volume induced by the drug at a concentration of IC_{50} for different compressive stresses. Like in the previous Figure, the first series of data serves as a control and indicates a variation of 50% with respect to the drug-free condition. The other series are related to the different compression regimes and compare the model response for the different mathematical relationships assumed for the death term. It is possible to observe that the variation in volume reduction is similar to the linear case, analyzed in the previous section. The effect of mechanical compression on drug efficacy described previously does not seem therefore to be originated from the particular mathematical form adopted for the death term.

Table 2
Parameter values for the relations assumed in the cell death term.

Relation	Parameter	Value	Unit	IC_{50}
Linear	λ_{ch}^{t}	5.0×10^{4}	$kg/(m^3 \cdot s)$	1.185×10^{-7}
Michaelis–Menten	m_1	1.5×10^{-2}	$kg/(m^3 \cdot s)$	5.345×10^{-8}
	m_2	1.0×10^{-7}	$(-)$	
Power law	p_1	2.5×10^{11}	$kg/(m^3 \cdot s)$	1.862×10^{-7}
	p_2	2	$(-)$	

4. Conclusion

In this work, we introduce equations for drug transport and uptake by TCs in our previous mathematical model for avascular tumor growth. Then, we adapt the equations for the tumor spheroid case and test the effects of a proliferation targeting drug on spheroid growth curves. We observe a qualitative agreement between model results and experimental literature (Gong et al., 2015; Kim et al., 2010; Mikhail et al., 2013; Wang et al., 2013). Then, we simulate tumor spheroids undergoing mechanical com-

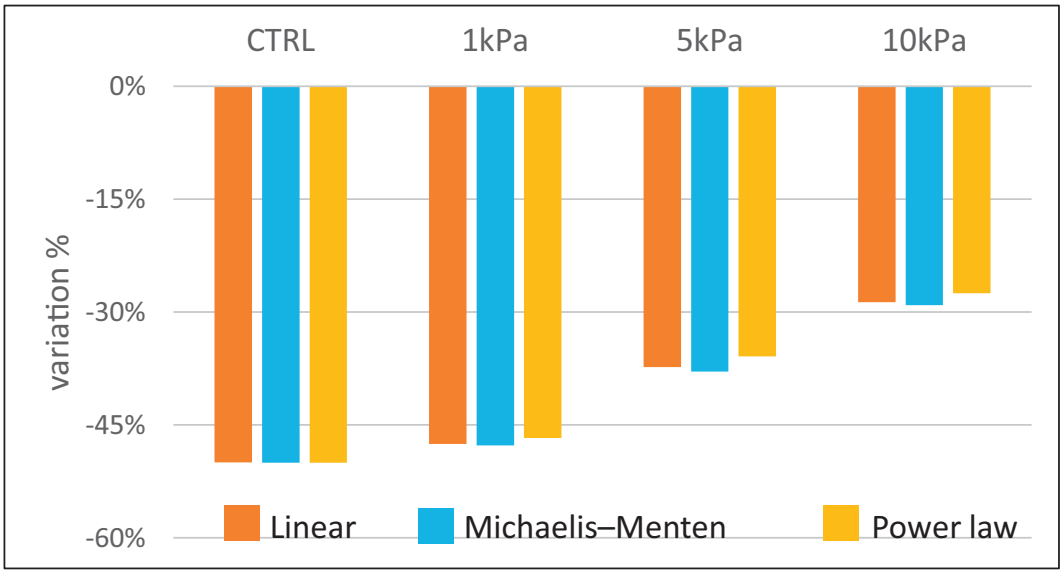

Fig. 9. Effect of different mathematical relations on spheroid volume variation. The drug concentration is selected according to the values of IC_{50} in Table 2.

pressive stresses of different amplitudes and consider their volume reduction due to the presence of a therapeutic agent. Interestingly, we notice a decreased growth inhibition efficacy of the drug in terms of the final volumes reached by the spheroids, arising because of compressive stresses. Finally, we test three different mathematical expressions for the cell death term induced by the therapeutic agent. The resulting predictions are similar for all the tested relations, suggesting that the particular form of the adopted constitutive relation does not influence model response. Taken together, these results suggest that mechanical compression of tumor spheroids may compromise the efficacy of a chemotherapeutic agent targeting cell proliferation.

As several simplifying assumptions are considered in the work, the model is certainly open to further improvements. In particular, here we model only one nutrient species, *i.e.* oxygen, diffusing in the interstitial fluid and regulating TC proliferation. Even though the presence of other chemicals is implicitly contained within the mass exchange term in (14), future inclusion of additional nutrients, growth and necrosis factors could provide a more detailed description of the tumor system (Chauhan and Jain, 2013; Jain et al., 2014). Moreover, since the particular physicochemical environment in which the tumor is embedded affects significantly the outcomes of therapies (see for example (Luk et al., 1990), (Seebacher et al., 2015)), proper consideration of these factors would result in a better description of drug dynamics. Notably, some experiments couple therapeutic agents to nanoparticle formulations, enabling a larger penetration into the tumor (Kim et al., 2010; Wang et al., 2013). Note that this latter kind of results can be integrated in the current model, once suitable mechanisms for nanoparticle delivery are hypothesized. As another remark, in this work we explicitly deal with drug delivery to avascular solid tumors. However, in the clinical practice, many chemotherapeutics are administered once the tumor has been vascularized – *i.e.* after tumor angiogenesis has taken place. In this case, the drug distribution is affected by several additional factors, such as the permeability of the vascular network (Boucher et al., 1990; Jain et al., 2007; Jain and Baxter, 1988), its tortuosity (Mascheroni and Penta, 2017; Penta and Ambrosi, 2015), and the amplitude of the interstitial pressure (Welter and Rieger, 2013; Wu et al., 2014).

Another point requiring some attention is the proper choice of constitutive relations. As it happens frequently in literature, most of these laws are derived from phenomenological arguments. More experimental work is needed to link the mathematical form assigned to the various terms to the underlying biology. This kind of reasoning should be applied to the constitutive relations accounting for the drug uptake and the following effects on TCs, as well as the mechanical description of the tumor ensemble. For the latter, here we consider a simple law, linking the stress in the tissue to the local volume fraction of tumor cells. This assumption provides a great simplification of the equations and is shown to give a good description of experimental observations (Mascheroni et al., 2016). However, it neglects several phenomena related to the mechanical behavior of a biological tissue. For example, viscoplastic effects existing at smaller timescales than those of cell proliferation are not taken into account (Forgacs et al., 1998; Giverso and Preziosi, 2012). Also, breaking and formation of cellular bonds during tumor development should be included to give a more complete description (Ambrosi et al., 2012; Preziosi et al., 2010). Finally, we highlight the need for experiments addressing the interactions between therapeutic agents and tumor mechanical environment. These experiments will serve to calibrate the parameters in the equations and to test model results. Part of future experimental work should also be devoted to the biochemical understanding of the growth inhibition process following mechanical stress. Although some work is already present in the literature (Cheng et al., 2009; Delarue et al., 2014; Loessner et al., 2013), several details remain to be elucidated. New investigations analyzing the interactions between the tumor and its bio-mechanical environment should allow for a better understanding of disease progression, with the final goal of aiding the design of effective therapeutic treatments.

Acknowledgements

BAS acknowledges the support of the Technische Universität München – Institute for Advanced Study, funded by the German Excellence Initiative and the European Union Seventh Framework Program under grant agreement no. 291763 and the support from NCI U54 CA210181. The research that lead to the present paper was also partially supported by a grant of the group GNFM of INdAM. The authors thank Luca Primo and Alberto Puliafito (Istituto di Candiolo, Italy) for valuable discussions.

References

Abercrombie, M., Ambrose, E.J., 1962. The surface properties of cancer cells: a review. Cancer Res 22, 525–548.

Altrock, P.M., Liu, L.L., Michor, F., 2015. The mathematics of cancer: integrating quantitative models. Nat. Rev. Cancer 15, 730–745. doi:10.1038/nrc4029.

Ambrosi, D., Preziosi, L., Vitale, G., 2012. The interplay between stress and growth in solid tumors. Mech. Res. Commun. 42, 87–91. doi:10.1016/j.mechrescom.2012.01.002.

Boucher, Y., Baxter, L.T., Jain, R.K., 1990. Interstitial pressure gradients in tissue-isolated and subcutaneous tumors: implications for therapy. Cancer Res 50, 4478–4484.

Butcher, D.T., Alliston, T., Weaver, V.M., 2009. A tense situation: forcing tumour progression. Nat. Rev. Cancer 9, 108–122. doi:10.1038/nrc2544.

Byrne, H., Preziosi, L., 2003. Modelling solid tumour growth using the theory of mixtures. Math. Med. Biol 20, 341–366. doi:10.1093/imammb/20.4.341.

Byrne, H.M., 2010. Dissecting cancer through mathematics: from the cell to the animal model. Nat. Rev. Cancer 10, 221–230. doi:10.1038/nrc2808.

Casciari, J.J., Sotirchos, S.V, Sutherland, R.M., 1992a. Mathematical modelling of microenvironment and growth in EMT6/Ro multicellular tumour spheroids. Cell Prolif 25, 1–22. doi:10.1111/j.1365-2184.1992.tb01433.x.

Casciari, J.J., Sotirchos, S.V, Sutherland, R.M., 1992b. Variations in tumor cell growth rates and metabolism with oxygen concentration, glucose concentration, and extracellular pH. J. Cell. Physiol. 151, 386–394. doi:10.1002/jcp.1041510220.

Chaplain, M.AJ., Graziano, L., Preziosi, L., 2006. Mathematical modelling of the loss of tissue compression responsiveness and its role in solid tumour development. Math. Med. Biol 23, 197–229. doi:10.1093/imammb/dql009.

Chauhan, V.P., Jain, R.K., 2013. Strategies for advancing cancer nanomedicine. Nat. Mater. 12, 958–962. doi:10.1038/nmat3792.

Cheng, G., Tse, J., Jain, R.K., Munn, L.L., 2009. Micro-environmental mechanical stress controls tumor spheroid size and morphology by suppressing proliferation and inducing apoptosis in cancer cells. PLoS One 4, e4632. doi:10.1371/journal.pone.0004632.

Curtis, L.T., England, C.G., Wu, M., Lowengrub, J., Frieboes, H.B., 2016. An interdisciplinary computational/experimental approach to evaluate drug-loaded gold nanoparticle tumor cytotoxicity. Nanomedicine 11, 197–216. doi:10.2217/nnm.15.195.

Dawidczyk, C.M., Kim, C., Park, J.H., Russell, L.M., Lee, K.H., Pomper, M.G., Searson, P.C., 2014. State-of-the-art in design rules for drug delivery platforms: lessons learned from FDA-approved nanomedicines. J. Control. Release 187, 133–144. doi:10.1016/j.jconrel.2014.05.036.

Delarue, M., Montel, F., Vignjevic, D., Prost, J., Joanny, J.-F., Cappello, G., 2014. Compressive stress inhibits proliferation in tumor spheroids through a volume limitation. Biophys. J. 107, 1821–1828. doi:10.1016/j.bpj.2014.08.031.

Dietrich, C., Wallenfang, K., Oesch, F., Wieser, R., 1997. Differences in the mechanisms of growth control in contact-inhibited and serum-deprived human fibroblasts. Oncogene 15, 2743–2747. doi:10.1038/sj.onc.1201439.

Fernández-Sánchez, M.E., Barbier, S., Whitehead, J., Béalle, G., Michel, A., Latorre-Ossa, H., Rey, C., Fouassier, L., Claperon, A., Brullé, L., Girard, E., Servant, N., Rio-Frio, T., Marie, H., Lesieur, S., Housset, C., Gennisson, J.-L., Tanter, M., Ménager, C., Fre, S., Robine, S., Farge, E., 2015. Mechanical induction of the tumorigenic β-catenin pathway by tumour growth pressure. Nature 523, 92–95. doi:10.1038/nature14329.

Forgacs, G., Foty, R.a, Shafrir, Y., Steinberg, M.S., 1998. Viscoelastic properties of living embryonic tissues: a quantitative study. Biophys. J. 74, 2227–2234. doi:10.1016/S0006-3495(98)77932-9.

Frieboes, H.B., Edgerton, M.E., Fruehauf, J.P., Rose, F.R.A.J., Worrall, L.K., Gatenby, R.a, Ferrari, M., Cristini, V., 2009. Prediction of drug response in breast cancer using integrative experimental/computational modeling. Cancer Res 69, 4484–4492. doi:10.1158/0008-5472.CAN-08-3740.

Friedrich, J., Seidel, C., Ebner, R., Kunz-Schughart, L.A., 2009. Spheroid-based drug screen: considerations and practical approach. Nat. Protoc. 4, 309–324. doi:10.1038/nprot.2008.226.

Galle, J., Preziosi, L., Tosin, A., 2009. Contact inhibition of growth described using a multiphase model and an individual cell based model. Appl. Math. Lett. 22, 1483–1490. doi:10.1016/j.aml.2008.06.051.
Giverso, C., Preziosi, L., 2012. Modelling the compression and reorganization of cell aggregates. Math. Med. Biol 29, 181–204. doi:10.1093/imammb/dqr008.
Gong, X., Lin, C., Cheng, J., Su, J., Zhao, H., Liu, T., Wen, X., Zhao, P., 2015. Generation of multicellular tumor spheroids with microwell-based agarose scaffolds for drug testing. PLoS One 10, e0130348. doi:10.1371/journal.pone.0130348.
Goodman, T.T., Chen, J., Matveev, K., Pun, S.H., 2008. Spatio-temporal modeling of nanoparticle delivery to multicellular tumor spheroids. Biotechnol. Bioeng. 101, 388–399. doi:10.1002/bit.21910.
Helmlinger, G., Netti, P.A., Lichtenbeld, H.C., Melder, R.J., Jain, R.K., 1997. Solid stress inhibits the growth of multicellular tumor spheroids. Nat. Biotechnol. 15, 778–783. doi:10.1038/nbt0897-778.
Hengst, L., Dulic, V., Slingerland, J.M., Lees, E., Reed, S.I., 1994. A cell cycle-regulated inhibitor of cyclin-dependent kinases. Proc. Natl. Acad. Sci. U. S. A 91, 5291–5295. doi:10.1073/pnas.91.12.5291.
Hossain, S.S., Hossainy, S.F.a., Bazilevs, Y., Calo, V.M., Hughes, T.J.R., 2012. Mathematical modeling of coupled drug and drug-encapsulated nanoparticle transport in patient-specific coronary artery walls. Comput. Mech. 49, 213–242. doi:10.1007/s00466-011-0633-2.
Jain, R.K., Baxter, L.T., 1988. Mechanisms of heterogeneous distribution of monoclonal antibodies and other macromolecules in tumors: Significance of elevated interstitial pressure. Cancer Res 48, 7022–7032.
Jain, R.K., Martin, J.D., Stylianopoulos, T., 2014. The role of mechanical forces in tumor growth and therapy. Annu. Rev. Biomed. Eng 16, 321–346. doi:10.1146/annurev-bioeng-071813-105259.
Jain, R.K., Tong, R.T., Munn, L.L., 2007. Effect of vascular normalization by antiangiogenic therapy on interstitial hypertension, peritumor edema, and lymphatic metastasis: insights from a mathematical model. Cancer Res 67, 2729–2735. doi:10.1158/0008-5472.CAN-06-4102.
Kim, M., Gillies, R.J., Rejniak, K.A,, 2013. Current Advances in Mathematical Modeling of Anti-Cancer Drug Penetration into tumor tissues. Front. Oncol. 3, 278. doi:10.3389/fonc.2013.00278.
Kim, T.-H., Mount, C.W., Gombotz, W.R., Pun, S.H., 2010. The delivery of doxorubicin to 3-D multicellular spheroids and tumors in a murine xenograft model using tumor-penetrating triblock polymeric micelles. Biomaterials 31, 7386–7397. doi:10.1016/j.biomaterials.2010.06.004.
Kim, Y., Stolarska, M.A., Othmer, H.G., 2011. The role of the microenvironment in tumor growth and invasion. Prog. Biophys. Mol. Biol. 106, 353–379. doi:10.1016/j.pbiomolbio.2011.06.006.
Lewis, R.W., Schrefler, B.A., 1998. The Finite Element Method in the Static and Dynamic Deformation and Consolidation of Porous Media. John Wiley.
Loessner, D., Flegg, J.A, Byrne, H.M., Clements, J.A, Hutmacher, D.W., 2013. Growth of confined cancer spheroids: a combined experimental and mathematical modelling approach. Integr. Biol. 5, 597. doi:10.1039/c3ib20252f.
Lowengrub, J.S., Frieboes, H.B., Jin, F., Chuang, Y.-L., Li, X., Macklin, P., Wise, S.M., Cristini, V., 2010. Nonlinear modelling of cancer: bridging the gap between cells and tumours. Nonlinearity 23, R1–R91. doi:10.1088/0951-7715/23/1/R01.
Luk, C.K., Veinot-Drebot, L., Tjan, E., Tannock, I.F., 1990. Effect of transient hypoxia on sensitivity to doxorubicin in human and murine cell lines. J. Natl. Cancer Inst. 82, 684–692. doi:10.1093/jnci/82.8.684.
Mascheroni, P., Penta, R., 2017. The role of the microvascular network structure on diffusion and consumption of anticancer drugs. Int. J. Numer. Method. Biomed. Eng e2857. doi:10.1002/cnm.2857.
Mascheroni, P., Stigliano, C., Carfagna, M., Boso, D.P., Preziosi, L., Decuzzi, P., Schrefler, B.A., 2016. Predicting the growth of glioblastoma multiforme spheroids using a multiphase porous media model. Biomech. Model. Mechanobiol. 15, 1215–1228. doi:10.1007/s10237-015-0755-0.
Mikhail, A.S., Eetezadi, S., Allen, C., 2013. Multicellular tumor spheroids for evaluation of cytotoxicity and tumor growth inhibitory effects of nanomedicines in vitro: a comparison of docetaxel-loaded block copolymer micelles and Taxotere®. PLoS One 8, e62630. doi:10.1371/journal.pone.0062630.
Montel, F., Delarue, M., Elgeti, J., Vignjevic, D., Cappello, G., Prost, J., 2012. Isotropic stress reduces cell proliferation in tumor spheroids. New J. Phys. 14, 55008. doi:10.1088/1367-2630/14/5/055008.
Mpekris, F., Angeli, S., Pirentis, A.P., Stylianopoulos, T., 2015. Stress-mediated progression of solid tumors: effect of mechanical stress on tissue oxygenation, cancer cell proliferation, and drug delivery. Biomech. Model. Mechanobiol. 14, 1391–1402. doi:10.1007/s10237-015-0682-0.
Mueller-Klieser, W., 2000. Tumor biology and experimental therapeutics. Crit. Rev. Oncol. Hematol. 36, 123–139.
Mueller-Klieser, W., Freyer, J.P., Sutherland, R.M., 1986. Influence of glucose and oxygen supply conditions on the oxygenation of multicellular spheroids. Br. J. Cancer 53, 345–353.
Mueller-Klieser, W.F., Sutherland, R.M., 1982. Oxygen tensions in multicell spheroids of two cell lines. Br. J. Cancer 45, 256–264.
Netti, P.A., Berk, D.A., Swartz, M.A., Grodzinsky, A.J., Jain, R.K., 2000. Role of extracellular matrix assembly in interstitial transport in solid tumors. Cancer Res 60, 2497–2503.
Penta, R., Ambrosi, D., 2015. The role of the microvascular tortuosity in tumor transport phenomena. J. Theor. Biol. 364, 80–97. doi:10.1016/j.jtbi.2014.08.007.
Pinder, G.F., Gray, W.G., 2008. Essentials of Multiphase Flow and Transport in Porous Media, 1st ed. John Wiley & Sons, Hoboken, New Jersey doi:10.1002/9780470380802.
Planas-Silva, M.D., Weinberg, R.A., 1997. The restriction point and control of cell proliferation. Curr. Opin. Cell Biol. 9, 768–772. doi:10.1016/S0955-0674(97)80076-2.
Polyak, K., Kato, J.Y., Solomon, M.J., Sherr, C.J., Massague, J., Roberts, J.M., Koff, A., 1994. p27Kip1, a cyclin-Cdk inhibitor, links transforming growth factor-beta and contact inhibition to cell cycle arrest. Genes Dev. 8, 9–22. doi:10.1101/gad.8.1.9.
Preziosi, L., Ambrosi, D., Verdier, C., 2010. An elasto-visco-plastic model of cell aggregates. J. Theor. Biol. 262, 35–47. doi:10.1016/j.jtbi.2009.08.023.
Preziosi, L., Tosin, A., 2009. Multiphase and multiscale trends in cancer modelling. Math. Model. Nat. Phenom. 4, 1–11. doi:10.1051/mmnp/20094301.
Sciumè, G., Gray, W.G., Ferrari, M., Decuzzi, P., Schrefler, B.A., 2013. On computational modeling in tumor growth. Arch. Comput. Methods Eng. 20, 327–352. doi:10.1007/s11831-013-9090-8.
Sciumè, G., Shelton, S., Gray, W., Miller, C., Hussain, F., Ferrari, M., Decuzzi, P., Schrefler, B., 2013. A multiphase model for three-dimensional tumor growth. New J. Phys. 15, 15005. doi:10.1088/1367-2630/15/1/015005.
Seebacher, N.A., Richardson, D.R., Jansson, P.J., 2015. Glucose modulation induces reactive oxygen species and increases P-glycoprotein-mediated multidrug resistance to chemotherapeutics. Br. J. Pharmacol. 172, 2557–2572. doi:10.1111/bph.13079.
St Croix, B., Florenes, V.A., Rak, J.W., Flanagan, M., Bhattacharya, N., Slingerland, J.M., Kerbel, R.S, 1996. Impact of the cyclin-dependent kinase inhibitor p27Kip1 on resistance of tumor cells to anticancer agents. Nat. Med. 2, 1204–1210.
St Croix, B., Sheehan, C., Rak, J.W., Florenes, V.A, Slingerland, J.M., Kerbel, R.S., 1998. E-Cadherin-dependent growth suppression is mediated by the cyclin-dependent kinase inhibitor p27(KIP1). J. Cell Biol 142, 557–571. doi:10.1083/jcb.142.2.557.
Stylianopoulos, T., Martin, J.D., Chauhan, V.P., Jain, S.R., Diop-Frimpong, B., Bardeesy, N., Smith, B.L., Ferrone, C.R., Hornicek, F.J., Boucher, Y., Munn, L.L., Jain, R.K., 2012. Causes, consequences, and remedies for growth-induced solid stress in murine and human tumors. Proc. Natl. Acad. Sci. 109, 15101–15108. doi:10.1073/pnas.1213353109.
Trédan, O., Galmarini, C.M., Patel, K., Tannock, I.F., 2007. Drug resistance and the solid tumor microenvironment. J. Natl. Cancer Inst. 99, 1441–1454. doi:10.1093/jnci/djm135.
Vinci, M., Gowan, S., Boxall, F., Patterson, L., Zimmermann, M., Court, W., Lomas, C., Mendiola, M., Hardisson, D., Eccles, S.A., 2012. Advances in establishment and analysis of three-dimensional tumor spheroid-based functional assays for target validation and drug evaluation.. BMC Biol 10, 29. doi:10.1186/1741-7007-10-29.
Wang, X., Zhen, X., Wang, J., Zhang, J., Wu, W., Jiang, X., 2013. Doxorubicin delivery to 3D multicellular spheroids and tumors based on boronic acid-rich chitosan nanoparticles. Biomaterials 34, 4667–4679. doi:10.1016/j.biomaterials.2013.03.008.
Ward, J.P., King, J.R., 2003. Mathematical modelling of drug transport in tumour multicell spheroids and monolayer cultures. Math. Biosci. 181, 177–207.
Weinberg, B.D., Patel, R.B., Exner, A.A., Saidel, G.M., Gao, J., 2007. Modeling doxorubicin transport to improve intratumoral drug delivery to RF ablated tumors. J. Control. Release 124, 11–19. doi:10.1016/j.jconrel.2007.08.023.
Welter, M., Rieger, H., 2013. Interstitial fluid flow and drug delivery in vascularized tumors: a computational model. PLoS One 8. doi:10.1371/journal.pone.0070395.
Wu, M., Frieboes, H.B., Chaplain, M.AJ., McDougall, S.R., Cristini, V., Lowengrub, J.S., 2014. The effect of interstitial pressure on therapeutic agent transport: coupling with the tumor blood and lymphatic vascular systems. J. Theor. Biol. 355, 194–207. doi:10.1016/j.jtbi.2014.04.012.
Xing, H., Wang, S., Hu, K., Tao, W., Li, J., Gao, Q., Yang, X., Weng, D., Lu, Y., Ma, D., 2005. Effect of the cyclin-dependent kinases inhibitor p27 on resistance of ovarian cancer multicellular spheroids to anticancer chemotherapy. J. Cancer Res. Clin. Oncol. 131, 511–519. doi:10.1007/s00432-005-0677-9.
Zahreddine, H., Borden, K.L.B., 2013. Mechanisms and insights into drug resistance in cancer. Front. Pharmacol. 4, 28. doi:10.3389/fphar.2013.00028.